

THEMAL PERFORMANCE INVESTIGATION OF AN ALUMINUM FANLESS THERMAL STORAGE INDOOR HEAT EXCHANGER UNDER MULTIPLE OPERATION PARAMETERS: AN EXPERIMENTAL AND NUMERICAL STUDY

SHAO Suola^{1*}, XU chengcheng²

¹ School of Civil Engineering and Architecture, Zhejiang Sci-Tech University, Hangzhou 310018, China, solar_shao@163.com

² College of Civil Engineering and Architecture, Zhejiang University of Water Resources and Electric Power, Hangzhou 310018, China, chengchengxu_seu@163.com,

* Corresponding author, solar_shao@163.com

The direct-condensation indoor heat exchanger was an effective heating method for winter heating. However, the metal thermal strength and pressure-bearing capacity of the previous steel panel were weaker than that of aluminum materials. Consequently, a novel aluminum fanless thermal storage indoor heat exchanger (AHE) is proposed for the air-source heat pump (ASHP) heating system. The model is established to explore the heating performances of the novel direct-condensation indoor heat exchanger. Compared with experimental data, the deviation of the predicted heat dissipation changes from -2.4% and 3.6%, verifying the model's reliability. To investigate the thermal potentials of the AHE under multiple operation parameters, a total of 66 cases were conducted. Results show that the ascendant condensation temperature and refrigerant flow rate are beneficial for the improvement of the heat exchange performance. Meanwhile, the increased condensation temperature also contributes to decreasing flow losses. In simulations, the average temperature difference between the refrigerant and panel surface is 9.7 °C. The maximum temperature difference of adjacent layers of the AHE is 6.3 °C, occurring between the copper tube and the water layer. Based on the simulated values, a thermolysis correlation was proposed for the AHE to predict the heat dissipation under multiple operation parameters. This study provides a stable and reliable direction-condensation heating terminal for ASHP systems. The results of this study are beneficial for the promotion and application of the direction-condensation heating terminal.

KEYWORDS: *Air source heat pump, Indoor heat exchanger, Model verification, Thermal performances, Thermolysis correlation.*

1. INTRODUCTION

The International Energy Agency predicts that the energy demand will grow by 30% in 2040. Countries are working together to address energy issues through various international agreements. The United States has put pressure on energy conservation and emission reduction through policies such as carbon tariffs, while the UK and Japan have introduced low-carbon energy bills. China pledged at the United Nations General Assembly to peak carbon emissions by 2030 and achieve carbon neutrality by 2060.

More and more low-emission and low-pollution technologies are being developed. Air source heat pump (ASHP), an environmentally friendly heating technology, is popular in space heating.

ASHP systems are often integrated with split air-conditioners to create a suitable artificial environment. However, the air supply speed of this indoor heat exchanger fluctuates during operation. Compared with other indoor heat exchangers, the predicted percentage of dissatisfaction of the ASHP with split air-conditioners exceeds 15%. In addition, the upper supply and lower return air supply method results in a large indoor vertical temperature gradient [4]. The temperature distribution of upper hot and lower cold is not in line with the thermal comfort laws [5]. Radiant heating terminals operate by transferring heat through radiation and, to a lesser extent, natural convection. This mechanism ensures even heat distribution and reduces energy consumption compared to conventional convective heating systems. To improve indoor thermal comfort, the radiant heating terminals have been integrated with ASHP systems for winter heating. However, traditionally, a water system is still needed as a medium between the ASHP system and the radiant heating terminal. The water in the water tank is heated by refrigerant, and then hot water is directed into the indoor radiators or radiant floors to heat indoor air [6]. The heating system undergoes secondary heat exchange, the condensation temperature is increased and energy efficiency is decreased. Xiao et al. [7] pointed out that when the outdoor temperature is between $-20\text{ }^{\circ}\text{C}$ and $-7\text{ }^{\circ}\text{C}$, the COP of the radiator heating system is 0.1~0.3 lower than that of the split air-conditioner heating system. Secondly, water pumps and tanks make the system more complex, causing more operational and maintenance burdens.

To avoid the above issues and further promote the advantages of radiant heating systems, direct-condensation indoor heat exchangers are proposed [8]. Zeng et al. [9] proposed a direct-condensation floor heating terminal integrated with ASHP system. The experimental results show that the system has good preheating performance, and its annual operating cost is 50% to 60% lower than that of the split air-conditioner heating system [10]. Dong et al. [11] pointed out that the direct-condensation floor heating system has long copper pipes, and high costs in later maintenance and operation. Therefore, they proposed a novel direct-condensation device. The fans are introduced inside the heat exchanger to enhance heat exchange performance. The author previously proposed a steel direct-condensation indoor heat exchanger [12]. The heat storage medium is introduced to the heat exchanger to maintain stable indoor temperature during defrosting conditions. The results show that the temperature difference between the heating rooms is below $3\text{ }^{\circ}\text{C}$, and the PMV/PPD index meets the international thermal comfort standard requirements.

Traditionally, radiant heating terminals have been constructed using steel due to its strength and thermal conductivity [13]. However, recent advancements in materials science and manufacturing have highlighted aluminum as a superior alternative for radiant heat exchanger construction [14]. Aluminum offers higher thermal conductivity, lighter weight, and better corrosion resistance compared to steel [15]. These properties not only enhance the heat transfer performance of the heat exchangers but also contribute to easier installation and longer service life. Additionally, aluminum's recyclability and environmental benefits further position it as a desirable material in the context of sustainable building technologies. Despite these advantages, the thermal performance of aluminum heat exchangers under varying operational conditions remains insufficiently explored, especially in conjunction with ASHP systems that directly supply refrigerant.

The investigation of thermal performance in such systems is critical for optimizing their design and operation [16]. Key parameters, including refrigerant flow rate, inlet temperature, and heat exchanger surface characteristics, significantly influence the heat transfer efficiency and overall system performance [17]. Experimental studies provide valuable insights into the real-world behavior of these systems, while numerical simulations offer a complementary approach to predict and analyze their thermal performance

under diverse operating conditions. By combining experimental and numerical methods, a comprehensive understanding of the system can be achieved, enabling the development of more efficient and reliable heating solutions. Such investigations not only inform the engineering community but also provide practical guidelines for industry stakeholders to adopt these innovative systems in both residential and commercial applications.

Previous studies have examined the performance of direct condensation heat exchanger systems and their integration with ASHP systems. Additionally, these studies have highlighted the importance of system design, including the placement and material selection of heat exchangers, to optimize performance. However, most of these investigations have focused on water-based radiant systems or heat exchangers made of traditional materials such as steel. Few studies have addressed the direct refrigerant supply to aluminum radiant heat exchangers and the associated thermal performance under multiple operational parameters.

This study proposed a novel, fanless, aluminum indoor heat exchanger (AHE) with thermal storage that can be integrated with ASHP systems. In order to investigate the thermal performance of AHE, a mathematical model suitable for flow heat transfer of AHE was established and its accuracy was verified. Based on the proposed mathematical model, the thermal performances of AHE under different operating parameters were investigated and the heat dissipation characteristic formulas of AHE under different operating parameters were proposed. This study aims to provide a detailed understanding of the AHE system, identify opportunities for performance optimization and provide a robust framework for evaluating and improving the thermal performance of aluminum radiant heat exchanger.

2. FANLESS ALUMINUM INDOOR HEAT EXCHANGER WITH THERMAL STORAGE

2.1 STRUCTURE OF AHE

The structural diagram of the AHE is shown in Figure 1. The indoor heat exchanger with a size of 1.6 m×0.65 m×0.15 m (L×H×T) is composed of 10 front columns and 10 rear columns. Each column has a width of 144 mm. The front plate of the front column is flat while the rear plate of the front column is equipped with parallel composite fins. Two sets of 2 cm high and 1 mm thick fins are installed on the front and rear plates of the rear columns. Sixty meters of copper pipes are arranged inside the heat exchanger. The copper tubes have been divided into four pipelines. Each line is 15 m long. 15 kg water is filled into the gap between the copper tube and the column as the heat storage medium.

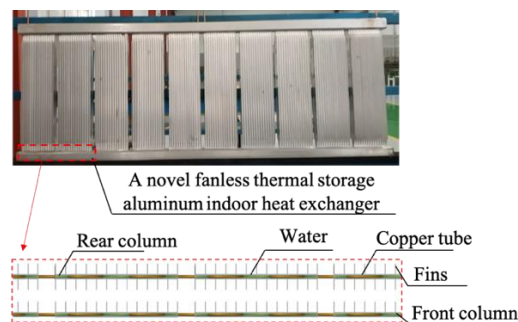
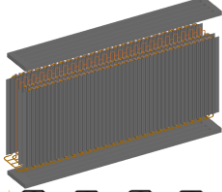
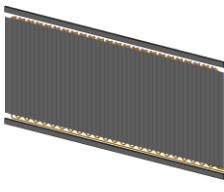
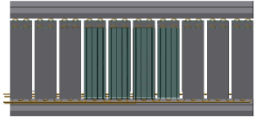
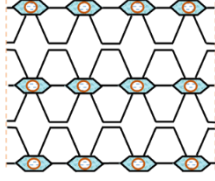
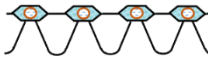
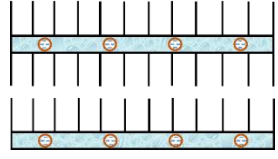


Figure 1: Structure of the AHE.

There are structural and material differences between the AHE proposed in this study and the steel radiant panel heat exchanger previously proposed by the authors [12, 18-20]. The differences in copper tube layout style, fin structure, channel version, etc. are shown in Table 1.

Table 1: Differences between the developed AHE and previous steel heat exchanger.

Type	Previous steel heat exchanger		Proposed AHE
3D structure diagram			
Partial transverse section diagram			
Channel version (Area×Wet circumference)	Hexagonal (128mm ² ×48.8mm)	Hexagonal (128mm ² ×48.8mm)	Large rectangular column (1008mm ² ×158mm)
Copper tube layout style Fin (Length×Span)	Full channel piping Composite fin (3cm×1cm)	Full channel piping Straight circular composite fin (3cm×1cm)	Four pipe line in one channel Parallel fins with a length of 2 cm

2.2 EXPERIMENTAL SYSTEM

Figure 2 shows a schematic diagram of the performance testing platform and measurement points layout for the AHE integrated with an ASHP system. As shown in Figure 2 (a), the experimental platform consists of two small chambers with dimensions of 4 m (L) × 4 m (W) × 3 m (H). To avoid the impact of the indoor air conditioning system on the velocity field, a testing chamber with dimensions of 3.5 m (L) × 3.5 m (W) × 2.5 m (H) is also built in the indoor chamber. The heating system mainly consists of an LG ASHP unit with a piston rotary compressor and an AHE, and uses R410A as the refrigerant.

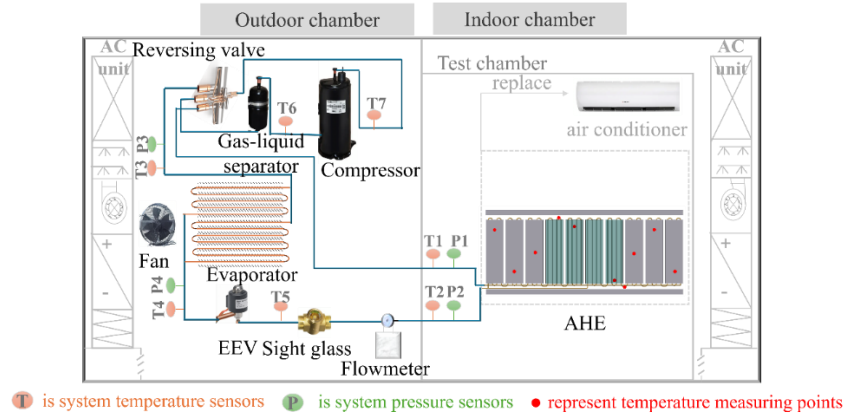


Figure 2: Schematic diagram of the performance testing platform

As shown in Figure 2, to measure the changes in various parameters, 4 pressure sensors and 7 temperature sensors are installed at the system to record the inlet and outlet pressure and temperature data of the refrigerant. To monitor the flow rate, a Coriolis force mass flowmeter is installed at the outlet of AHE. To observe the flow state of the refrigerant, a sight glass is connected behind the flow meter. A total of 11 temperature measurement points are arranged on the water layer, plate surface, and fins of AHE to monitor the temperature changes of AHE during the experiment. Similarly, to measure indoor air temperature, 5 temperature measurement points are set up in the center of the room at heights of 0.1 m, 0.75 m, 1.1 m, 2 m, and 2.4 m from the ground. To measure the temperature

changes of walls, a temperature measuring point is placed in the center of each of the 6 wall surfaces of the indoor chamber.

2.3 MATHEMATICAL MODEL

The novel AHE is composed of the refrigerant fluid (re), the copper tube (co), the water layer (wa), the aluminum plate (ap), and the fins (fi). To facilitate the solution, simplifications and assumptions were made in the heat transfer model: 1) The materials are homogeneous and in tight contact. 2) Neglect the natural flow of the water caused by temperature differences. 3) Neglect the heat conduction between adjacent nodes along the refrigerant flow direction. 4) Disconnect the heat exchange column from the middle and treat it as a separate control unit. 5) Equivalent the channels to concentric circles. 6) The indoor air temperature and wall temperature remain constant.

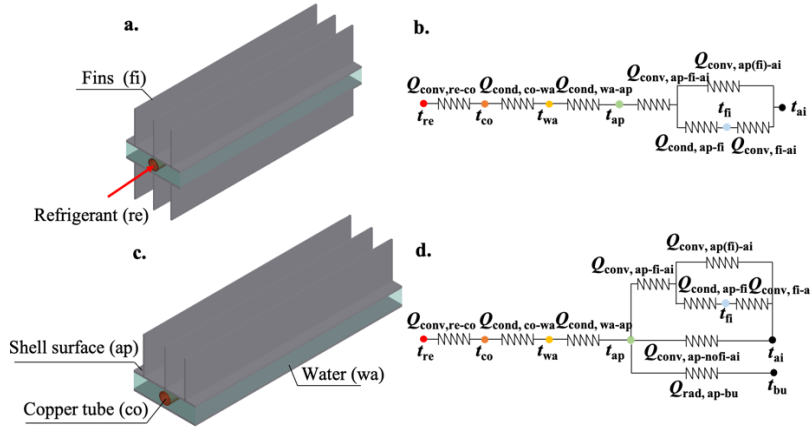


Figure 3: The heat transfer mechanism of the AHE: rear column microelement (a), heat transfer mechanism of rear column (b), front column microelement (c), and heat transfer mechanism of front column (d).

Figure 3 shows the control volume division of the AHE. The front and rear columns are divided into "i" control volumes ($1 \leq i \leq n$). Due to structural differences and position differences between the front column and the rear column, the heat transfer processes of the two columns are shown in Figure 3 (b) and (d).

The equilibrium equations for the control volume "i" ($1 \leq i \leq n$) in the mathematical model are listed as follows:

$$\Delta P_{re}(i) = \Delta P_g(i) + \Delta P_m(i) + \Delta P_f(i) \quad (1)$$

$$Q_{re}(i) - Q_{conv, re-co}(i) = 0 \quad (2)$$

$$Q_{conv, re-co}(i) - Q_{cond, co-wa}(i) = 0 \quad (3)$$

$$Q_{cond, co-wa}(i) - Q_{cond, wa-ap}(i) = 0 \quad (4)$$

$$Q_{cond, wa-ap}(i) - Q_{conv, ap-ai}(i) - Q_{rad, ap-bu}(i) = 0 \quad (5)$$

$$Q_{conv, ap-ai}(i) - Q_{conv, ap-nof-i-ai}(i) - Q_{conv, ap-fi-ai}(i) = 0 \quad (6)$$

$$Q_{conv, ap-fi-ai}(i) - Q_{conv, ap(fi)-ai}(i) - Q_{cond, ap-fi}(i) = 0 \quad (7)$$

where ΔP_{re} , ΔP_g , ΔP_m , and ΔP_f are the total flow loss, the gravitational pressure drop, the momentum pressure drop, and the friction pressure drop, respectively. Q_{re} is the heat transfer of refrigerant, $Q_{conv, re-co}$ is the thermal conductivity between refrigerant and copper tube, $Q_{cond, co-wa}$ is the thermal conductivity between copper tube and water layer, $Q_{cond, wa-ap}$ is the thermal conductivity between water layer and shell, $Q_{conv, ap-ai}$ is the convective heat transfer between the entire shell (including fins) and indoor air, $Q_{rad, ap-bu}$ is

the radiative heat transfer between the shell and enclosure structure, $Q_{\text{conv, ap-nof-i-ai}}$ is the convective heat transfer between the shell without fins and indoor air, $Q_{\text{conv, ap-fi-ai}}$ is the convective heat transfer between the shell with fins and indoor air, $Q_{\text{conv, ap(fi)-ai}}$ is the heat transfer between the shell (excluding the area occupied by fins) and indoor air, $Q_{\text{cond, ap-fi}}$ is the heat transfer between the shell and fins. In addition, empirical correlations related to the equilibrium equations are listed in Table 2.

Table 2: The correlations in the AHE model

Type	correlations
Q_{re}	$Q_{\text{re}}(i) = G_{\text{re}}(i) \times (h_{\text{re-in}}(i) - h_{\text{re-out}}(i))$
	$Q_{\text{conv, re-co}}(i) = A_{\text{co-in}}(i) \alpha_{\text{conv, re-co}}(i) \left(\frac{t_{\text{re-in}}(i) + t_{\text{re-out}}(i)}{2} - t_{\text{co-in}}(i) \right)$
	$Nu_{\text{conv, re-co}}(i) = \frac{(f_{\text{re-g}}(i)/8) Re_{\text{re-g}}(i) Pr_{\text{re-g}}(i)}{1 + 12.7 \sqrt{\frac{f_{\text{re-g}}(i)}{8}} (Pr_{\text{re-g}}(i)^{2/3} - 1)} \left[1 + \frac{d_{\text{co-in}}}{\Delta l} \right] \left(\frac{T_{\text{re}}(i)}{T_{\text{co-in}}(i)} \right)^{0.45} \quad [21]$
	$f_{\text{re-g}}(i) = (1.82 \lg Re_{\text{re-g}}(i) - 1.64)^2 \quad Re_{\text{re-g}}(i) = \frac{G_{\text{re}}(i) d_{\text{co-in}}}{\mu_{\text{re-g}}(i)}$
$Q_{\text{conv, re-co}}$	$Nu_{\text{conv, re-co}}(i) = \frac{(f_{\text{re-l}}(i)/8) Re_{\text{re-l}}(i) Pr_{\text{re-l}}(i)}{1 + 12.7 \sqrt{\frac{f_{\text{re-l}}(i)}{8}} (Pr_{\text{re-l}}(i)^{2/3} - 1)} \left[1 + \frac{d_{\text{co-in}}}{\Delta l} \right] \left(\frac{Pr_{\text{re}}(i)}{Pr_{\text{co-in}}(i)} \right)^{0.11} \quad [22]$
	$f_{\text{re-l}}(i) = [1.82 \lg Re_{\text{re-l}}(i) - 1.64]^2 \quad Re_{\text{re-l}}(i) = \frac{G_{\text{re}}(i) d_{\text{co-in}}}{\mu_{\text{re-l}}(i)}$
	$Nu_{\text{conv, re-co}}(i) = 0.023 Re_{\text{re}}(i)^{0.8} Pr_{\text{re}}(i)^{0.3}$
	$Nu_{\text{conv, re-co}}(i) = \left[\frac{(0.31 Re_{\text{re-ls}}(i)^{-1.32} + \frac{Re_{\text{re-ls}}(i)^{2.4} Pr_{\text{re-l}}(i)^{3.9}}{2.37 \times 10^{14}})^{1/3}}{+ \frac{Pr_{\text{re-l}}(i)^{1.3} 0.252 \mu_{\text{re-l}}(i)^{1.177} \mu_{\text{re-g}}(i)^{0.156}}{771.6 d_{\text{co-in}}^2 \rho_{\text{re-l}}(i)^{0.553} \rho_{\text{re-g}}(i)^{0.78}} (Re_{\text{re-l}}(i) - Re_{\text{re-ls}}(i))^{1.4} Re_{\text{re-ls}}(i)^{0.4}} \right]^{1/2} \quad [23]$
	$Re_{\text{re-ls}}(i) = \frac{G_{\text{re}}(i) \times (1 - x_{\text{re}}(i)) d_{\text{co-in}}}{\mu_{\text{re-l}}(i)}$
$Q_{\text{cond, co-wa}}$	$Q_{\text{cond, co-wa}}(i) = \Delta l \frac{t_{\text{co}}(i) - t_{\text{wa}}(i)}{\frac{1}{2\pi\lambda_{\text{co}}} \ln \frac{d_{\text{co-out}}}{d_{\text{co-in}}} + \frac{1}{2\pi\lambda_{\text{wa}}} \ln \frac{(d_{\text{ap-in}} + d_{\text{co-out}})/2}{d_{\text{co-out}}}} \quad [24]$
$Q_{\text{cond, wa-ap}}$	$Q_{\text{cond, wa-ap}}(i) = \Delta l \frac{t_{\text{wa}}(i) - t_{\text{ap}}(i)}{\frac{1}{2\pi\lambda_{\text{wa}}} \ln \frac{d_{\text{ap-in}}}{(d_{\text{ap-in}} + d_{\text{co-out}})/2} + \frac{1}{2\pi\lambda_{\text{ap}}} \ln \frac{d_{\text{ap-out}}}{d_{\text{ap-in}}}}$
$Q_{\text{rad, ap-bu}}$	$Q_{\text{rad, ap-bu}}(i) = \begin{cases} 5.67 \times 10^{-8} \times A_{\text{ap}} \times [(t_{\text{ap}}(i) + 273.15)^4 - (T_{\text{AUST}} + 273.15)^4] & \text{Front columns} \\ 0 & \text{Rear columns} \end{cases}$
	$T_{\text{AUST}} = \frac{\sum_1^6 A_i T_i}{\sum_1^6 A_i}$
$Q_{\text{conv, ap-nof-i-ai}}$	$Q_{\text{conv, ap-nof-i-ai}}(i) = A_{\text{ap-nof-i}}(i) \alpha_{\text{conv, ap-ai}}(i) (t_{\text{ap}}(i) - t_{\text{ai}}(i))$
	$A_{\text{ap-nof-i}} = \begin{cases} \Delta l \times L_{\text{ap}} & \text{Front columns} \\ 0 & \text{Rear columns} \end{cases}$
	$\alpha_{\text{conv, ap-ai}}(i) = \frac{Nu_{\text{conv, ap-ai}}(i) k_{\text{ai}}(i)}{\Delta l} \quad Nu_{\text{conv, ap-ai}}(i) = \left[0.825 + \frac{0.387 Ra_{\text{H}}(i)^{1/6}}{[1 + (0.492/Pr(i))^{9/16}]^{8/27}} \right]^2 \quad [25]$
	$Ra_{\text{H}}(i) = Pr(i) \frac{g \beta(i) \Delta l \theta(i)^3}{\nu(i)^2} \quad \theta(i) = t_{\text{ap}}(i) - t_{\text{ai}}(i) \quad \beta(i) = 1/(t_{\text{ai-f}}(i) + 273.15) \quad t_{\text{ai-f}}(i) = \frac{t_{\text{ai}}(i) + t_{\text{ap}}(i)}{2}$
	$Q_{\text{conv, ap-fi-ai}}(i) = \alpha_{\text{conv, ap-fi-ai}}(i) S_{\text{fi}} \left(\frac{t_{\text{ap}}(i) + t_{\text{fi-out}}(i)}{2} - t_{\text{ai}}(i) \right) \quad [26]$
	$S_{\text{fi}} = \Delta l W_{\text{fi}} + 2 n_{\text{fi}} L_{\text{fi}} \Delta l \quad \alpha_{\text{conv, ap-fi-ai}} = Nu_{\text{conv, ap-fi-ai}} \frac{\lambda_{\text{fi}}}{\sqrt{S_{\text{fi}}}}$
$Q_{\text{conv, ap-fi-ai}}$	$Nu_{\text{conv, ap-fi-ai}} = Nu_{\sqrt{S_{\text{fi}}}}^{\infty} + f(Pr) G_{\sqrt{S_{\text{fi}}}} Ra_{\sqrt{S_{\text{fi}}}}^{1/4} \quad Nu_{\sqrt{S_{\text{fi}}}}^{\infty} = \frac{3.192 + 1.868 \left(\frac{\delta_{\text{ap}} + L_{\text{fi}}}{\Delta l} \right)^{0.76}}{\sqrt{1 + 1.189 \frac{(\delta_{\text{ap}} + L_{\text{fi}})}{\Delta l}}}$
	$G_{\sqrt{S_{\text{fi}}}} = 1.0904 \left[\frac{\Delta l (n_{\text{fi}} L_{\text{fi}} + \delta_{\text{fi}} + W_{\text{fi}})^2}{(n_{\text{fi}} \delta_{\text{fi}} L_{\text{fi}} + \delta_{\text{fi}} W_{\text{fi}} + \Delta l (n_{\text{fi}} L_{\text{fi}} + \delta_{\text{fi}} + W_{\text{fi}}))^{3/2}} \right]^{1/4}$

$$\begin{aligned}
Ra_{\sqrt{s_n}} &= Pr \frac{g\beta \left[\frac{t_{ap}(i)+t_{fi-out}(i)}{2} - t_{ai} \right] (\sqrt{s_{fi}})^3}{\nu^2} \\
\beta &= 1 / \left[\left(\frac{t_{ap}(i)+t_{fi-out}(i)}{2} + t_{ai} + 273.15 \right) / 2 \right] \quad f(Pr) = 0.67 / [1 + (0.5/Pr)^{9/16}]^{4/9} \\
Q_{conv, ap(fi)-ai} &= A_{ap(fi)}(i) \alpha_{conv, ap-ai}(i) (t_{ap}(i) - t_{ai}(i)) \\
A_{ap(fi)} &= \begin{cases} \Delta l \times L_{ap} - n_{fi} \times \Delta l \times \delta_{fi} & \text{Front columns} \\ 2 \times \Delta l \times L_{ap} - 2 \times n_{fi} \times \Delta l \times \delta_{fi} & \text{Rear columns} \end{cases} \\
Q_{cond, ap-fi} &= A_{fi} \lambda_{fi} \frac{(t_{ap}(i) - t_{fi-out}(i))}{\delta_{fi}} \\
A_{fi} &= \begin{cases} n_{fi} \times \Delta l \times \delta_{fi} & \text{Front columns} \\ 2 \times n_{fi} \times \Delta l \times \delta_{fi} & \text{Rear columns} \end{cases} \\
\Delta P_m(i) &= G_{re}^2 \left(\frac{x_{re}(i)^2}{\xi \rho_{re-g}(i)} + \frac{(1-x_{re}(i))^2}{(1-\xi) \rho_{re-l}(i)} \right)_{out} - G_{re}^2 \left(\frac{x_{re}(i)^2}{\xi \rho_{re-g}(i)} + \frac{(1-x_{re}(i))^2}{(1-\xi) \rho_{re-l}(i)} \right)_{in} \quad [27,28] \\
\Delta P_m &= 1 - \frac{2(1-x_{re}(i))^2}{1-2x_{re}(i) + [1+4x_{re}(i)(1-x_{re}(i)) \left(\frac{\rho_{re-l}(i)}{\rho_{re-g}(i)} - 1 \right)]^{0.5}} \\
\Delta P_f(i) &= - \frac{2f(i)G_{re}^2 \Delta l}{d_{co-in} \rho_{re}(i)} \quad f(i) = 0.0046 Re_{re}(i)^{-0.2} \\
\Delta P_f(i) &= \Delta P_{f-l}(i) \phi(i)^2 \quad \phi(i)^2 = 1 + \frac{C}{\psi} + \frac{1}{\psi^2} \quad \psi^2 = \frac{\left(\frac{dP_f}{dz} \right)_l}{\left(\frac{dP_f}{dz} \right)_g} \\
\left(\frac{dP_f}{dz} \right)_l &= \frac{2f(i)G_{re}^2 (1-x_{re}(i))^2}{d_{co-in} \rho_{re-l}(i)} \quad \left(\frac{dP_f}{dz} \right)_g = \frac{2f(i)G_{re}^2 x_{re}(i)^2}{d_{co-in} \rho_{re-g}(i)} \quad [29] \\
C &= \begin{cases} 0.39 Re_{re-l}^{0.03} La_{re-g}^{0.1} \left(\frac{\rho_{re-l}}{\rho_{re-g}} \right)^{0.35} & Re_{re-l} \geq 2000, Re_{re-g} \geq 2000 \\ 8.7E-04 Re_{re-l}^{0.17} La_{re-g}^{0.5} \left(\frac{\rho_{re-l}}{\rho_{re-g}} \right)^{0.14} & Re_{re-l} \geq 2000, Re_{re-g} < 2000 \\ 0.0015 Re_{re-l}^{0.59} La_{re-g}^{0.19} \left(\frac{\rho_{re-l}}{\rho_{re-g}} \right)^{0.36} & Re_{re-l} < 2000, Re_{re-g} \geq 2000 \\ 3.5E-05 Re_{re-l}^{0.44} La_{re-g}^{0.5} \left(\frac{\rho_{re-l}}{\rho_{re-g}} \right)^{0.48} & Re_{re-l} < 2000, Re_{re-g} < 2000 \end{cases}
\end{aligned}$$

The calculation process is divided into three steps: 1) Input basic parameters, determine the inlet refrigerant state, and select the corresponding calculation area. 2) Select the corresponding empirical formulas and calculate the parameters using the joint equations (1)~(7). 3) Repeat step 2 until the total length of the control body reaches the copper tube length in AHE, stop calculating and output all values.

3. RESULTS AND DISCUSSION

3.1 EXPERIMENTAL RESULTS

Figure 4 shows the experimental results of thermal comfort and system heating efficiency. Figure 4 (a) shows the vertical temperature distribution of AHE compared to traditional split air-conditioners and steel heat exchangers previously proposed by authors[12,18-20], indicating that the indoor temperature distribution provided by the AHE is more uniform. The maximum temperature difference in the working area height (0.1-2 m) during AHE system heating is 3 °C. Figure 4 (b) shows that when the outdoor temperature is -7 °C, the condensation temperature of AHE increases from 40.7 °C to 47.4 °C, and the COP decreases from 2.50 to 1.98. Compared with the steel heat exchanger, the efficiency of AHE system is higher. Therefore, from the perspectives of thermal comfort and thermal efficiency, The AHE is competitive in existing heating systems.

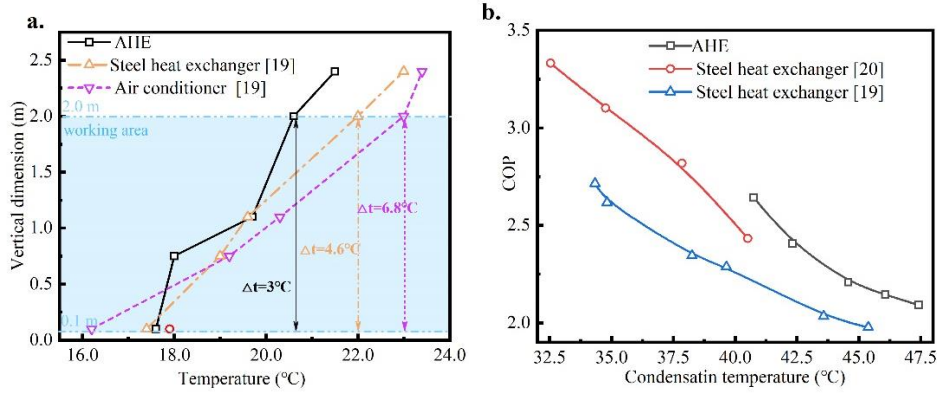


Figure 4: Experimental results of thermal comfort and system heating efficiency: indoor temperature variation (a), and COP performance (b).

3.2 SIMULATION VERIFICATION

The experimental data listed in Table 3. are input values for the mathematical model. The comparisons of numerical and experimental results are shown in Figure 5.

Table 3: Input value of the mathematical model.

Experimental data		Case 1	Case 2	Case 3	Case 4	Case 5
T_{re_in} (°C)		50.8	52.9	56.1	59.1	62.9
$T_{con_re_in}$ (°C)		43.3	44.8	46.9	48.5	50.9
P_{re_in} (kPa)		2619.3	2711.3	2849.3	2957.3	3124.3
G_{re_total} (kg/h)		45.4	45.7	48.8	54.4	56.7
T_{indoor} (K)	T_{ai}	18.4	18.2	18.1	18.1	18.0
	T_{wall_south}	17.6	18.2	17.9	17.7	17.8
	T_{wall_east}	17.5	18.2	18.0	17.7	17.8
	T_{wall_west}	17.6	18.1	18.0	17.7	17.8
	T_{wall_north}	20.5	20.6	20.5	20.7	20.2
	$T_{ceiling}$	19.6	18.1	18.1	18.4	18.2
	T_{floor}	17.7	18.3	18.0	17.9	17.9
	T_{AUST}	18.5	18.6	18.4	18.4	18.3

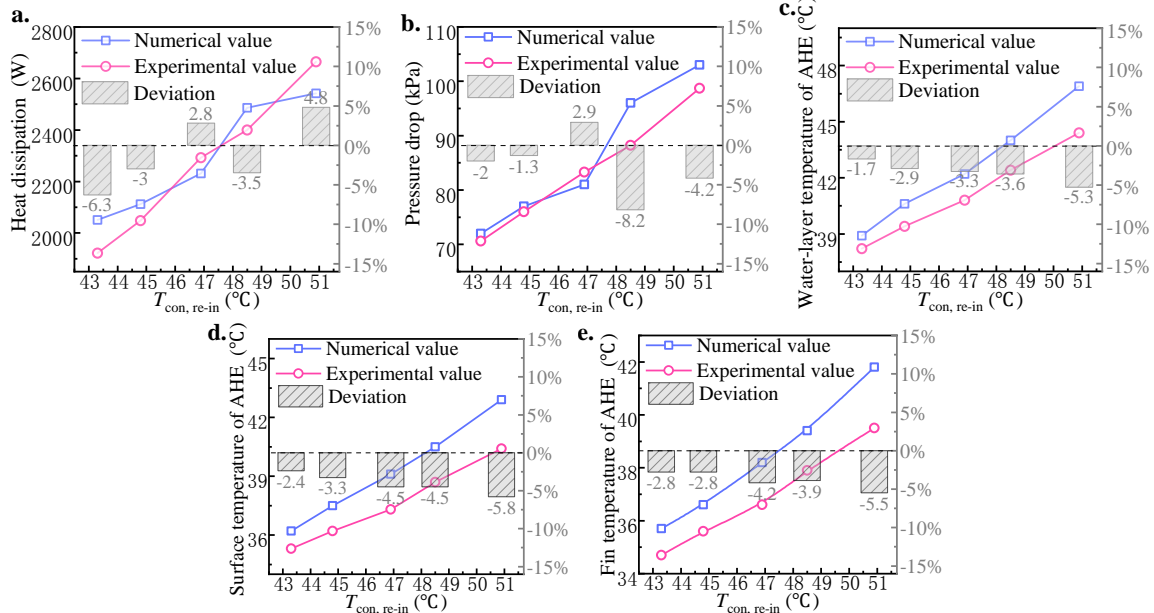


Figure 5: Comparisons of numerical and experimental results: heat dissipation (a), pressure drop (b), average water-layer temperature (c), average surface temperature (d), and average fin temperature (e).

Case 3 is the typical heating condition with a condensation temperature of 46.9 °C. The experimental heat flux is as high as 2144.5 W/m². As shown in Figure 3, the deviation between the simulated heat dissipation (Q) and experimental Q changes from -6.3% to 4.8% with a mean absolute value of 4.1%.

The deviation of pressure drop (ΔP_{re}) changes from -8.2% to 2.9%, with a mean absolute value of 3.7%. The deviation of water layer temperature (t_{wa}) is between -5.3% and -1.7%, with a mean absolute value of -3.4%. The deviation of the average temperature of the panel surface (t_{ap}) is between -5.8% and -2.4%, with a mean absolute value of 4.2%. The deviation of the average temperature of the fins (t_{fi-out}) is between -5.5% and -2.8%, with a mean absolute value of 3.8%. The experimental temperatures of each structural layer of AHE are higher than the simulated data. The main reason for this phenomenon is that the average temperature in the experiment was calculated through arranged data points, which is influenced by the position of the measurement points. In addition, the model ignores the mutual heat transfer between the front and rear columns, which may also result in higher experimental temperatures for AHE. The deviations between simulated and experimental values are all below 5%, demonstrating the effectiveness of the mathematical model.

3.3 THERMAL PERFORMANCE OF THE AHE

In Table 4, a total of 66 simulation cases are conducted to investigate the effects of operating parameters and indoor environmental parameters on the thermal performances of the AHE. The bold parameters are the main control variables.

Table 4: Ranges of operating parameters in numerical cases.

Main research variables	T_{re-in} (°C)	$T_{con, re-in}$ (°C)	P_{re-in} (kPa)	G_{re} (kg/h)	Δt_{re-in} (°C)	t_{ai} (°C)	t_{AUST} (°C)
Refrigerant flow rate	49	45	2726.1	32~36	4	18~22	16
Inlet condensation temperature	52-55	48~51	2924.5~3133.9	42	4	18~22	16
Imported overheating of inlet refrigerant	47-55	45	3431.3	47	2~10	18~22	16
Indoor enclosure structure temperatures	49	45	2726.1	38	4	20	14~18
	54	50	3062.8	42	4	20	14~18
	59	55	3431.3	47	4	20	14~18

The thermal performances of the AHE under different G_{re} are shown in Figure 6 (a). As G_{re} increases, the ΔP_{re} increases. When G_{re} changes from 32 kg/h to 36 kg/h, the average increment of ΔP_{re} is 13.1 kPa and the average growth rate is 3.27 kPa/(kg·h⁻¹). The added G_{re} contributes to the turbulent flow of the refrigerant fluid, resulting in the increased frictional pressure drop and momentum pressure drop. Similarly, the increased G_{re} will lead to the increased Q .

In Figure 6 (b), as the P_{re-in} increases from 2924.5 kPa to 3133.9 kPa, the Q of the AHE increases from 2047.9 W to 2116.8 W, with an increment of 68.9 W at the t_{ai} of 18 °C. When the t_{ai} rises from 18 °C to 22 °C, the average increase in Q is 96.7 W. On the other hand, the length of the single-phase subcooling region is added for improved heat exchange efficiency. Correspondingly, the t_{re-out} decreases. At the same time, the added length of the single-phase subcooled region is beneficial for reducing liquidity losses, resulting in a decrease in ΔP_{re} . As shown in Figure 6 (b), the ΔP_{re} and the t_{re-out} decrease with the added P_{re-in} . As the P_{re-in} increases from 2924.5 kPa to 3133.9 kPa, the average decrease of t_{re-out} is 4.9 °C while the average decrease of ΔP_{re} is 11.2 kPa.

The effects of import superheat (Δt_{re-in}) on the thermal performances are shown in Figure 6 (c). When the Δt_{re-in} increases from 2 °C to 10 °C, the average Q , the ΔP_{re} , and the t_{re-out} of the AHE increase by 152.3 W, 4.5 kPa, and 2.8 °C. The average growth rates are 19.0 W/°C, 0.56 kPa/°C, and 8.5%, respectively.

In Figure 6 (d), the indoor air temperature is 20 °C while the comprehensive temperature of the enclosure structure (t_{AUST}) changes from 14 °C to 18 °C. As t_{AUST} changed from 14 °C to 18 °C, the Q decreased by 14.5 W, ΔP_{re} increased by 0.5 kPa and t_{re-out} increased by 0.7 °C. From the heat transfer in the microelement, the higher indoor temperature leads to weaker heat exchange. Under the same refrigerant flow rate and inlet temperature, the length of the single-phase overheated region and the length of the two-phase flow region are increased while the length of the single-phase subcooled

region is decreased. Correspondingly, the t_{re-out} will be enhanced under the higher indoor temperatures. Similarly, the length proportion of the gaseous refrigerant flow region in the AHE increases, increasing the ΔP_{re} .

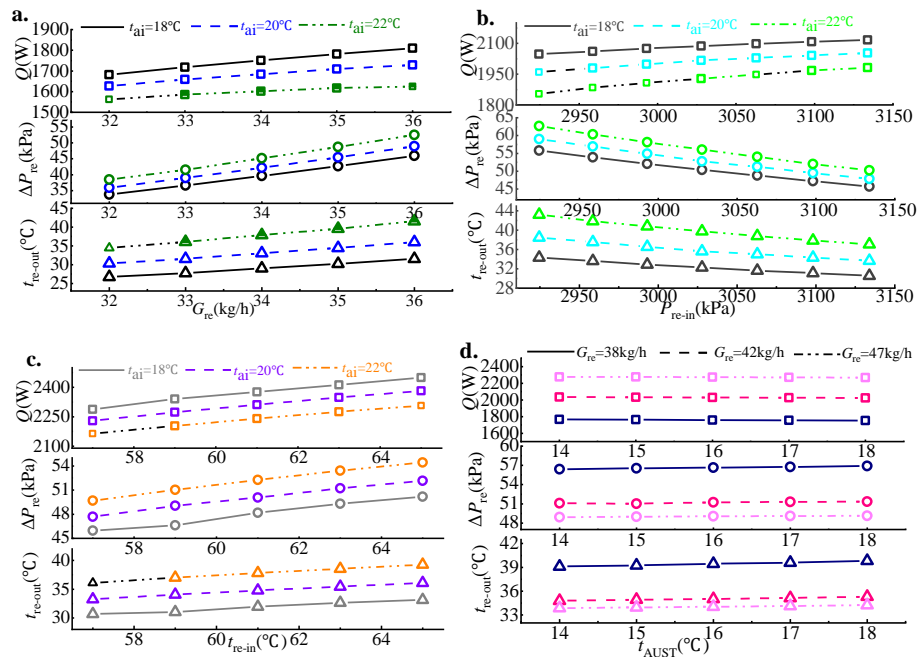


Figure 6: Thermal performance variations of the AHE under different operation parameters: effects of G_{re} (a), effects of P_{re-in} (b), effects of Δt_{re-in} (c), and effects of t_{AUST} (d).

The change rate of the Q , the ΔP_{re} , and the t_{re-out} under different operating parameters indicate that the condensation temperature and the refrigerant flow rate have a significant impact on thermal performance, followed by the import superheat degree and the indoor temperatures. In addition, the increased condensation temperature not only improves the heat dissipation but also reduces flow losses.

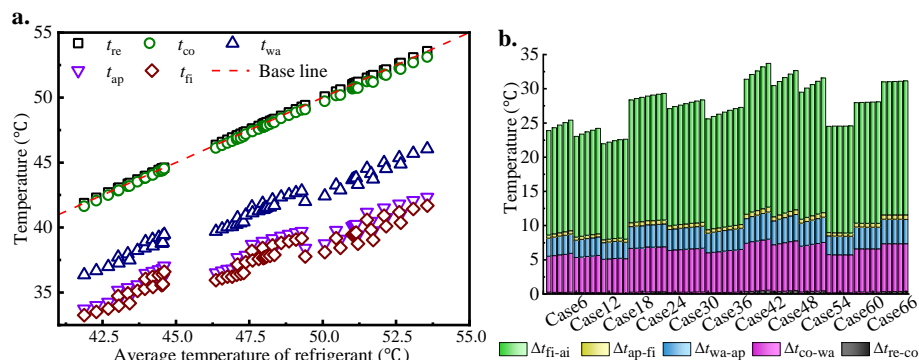


Figure 7: AHE temperatures analysis in 66 numerical cases: temperatures of each layer (a) and temperature differences between adjacent layers (b).

Figure 7 indicates that the higher t_{re} , the higher the temperature of the AHE. In 66 simulation cases, the average t_{re} of the AHE fluctuates between 41.9 °C and 53.6 °C, the temperature of the copper tube ranges from 41.6 °C to 53.1 °C, the average temperature of the water layer ranges from 36.4 °C to 46.0 °C, the average temperature of the panel surface ranges from 33.7 °C to 42.3 °C, and the average temperature of the fin-end ranges from 32.3 °C to 41.7 °C. As shown in Figure 7 (a), the temperature difference between the refrigerant and the copper tube (Δt_{re-co}) is between 0.07 °C and 0.54 °C, with an average temperature difference of 0.26 °C. The average temperature difference between the

refrigerant and the water layer (Δt_{re-wa}), the Δt_{re-ap} , the Δt_{re-fi} , and the Δt_{re-ai} is 6.5 °C, 9.6 °C, 10.2 °C, and 27.7 °C, respectively. In addition, Figure 7 shows that the panel surface temperature and the fin-end temperature are very close, with an average temperature difference of 0.56 °C. The temperature differences between the copper tube and the water layer (Δt_{co-wa}), the Δt_{wa-ap} , and the Δt_{fi-ai} are relatively large, with an average temperature difference of 6.2 °C, 3.1 °C, and 17.5 °C, respectively. The results indicate that the thermal performances of the AHE can be improved by reducing the thickness of the water layer and increasing the length of the fins.

Figure 8 (a) shows the effect of pressure drop on heat dissipation and compares the heat dissipation of AHE considering and ignoring the pressure drop effect. The results show that when the pressure drop ranges from 33.8kPa to 62.6kPa, the heat dissipation of AHE without considering the pressure drop increased by a very small margin compared to that considering the pressure drop, with an average increase of only 0.025%. However, for the outlet condensation temperature, considering the effect of pressure drop reduces it by about 1 °C compared to ignoring pressure drop, with an average deviation of 1.7%. Therefore, the pressure drop of AHE has little effect on heat dissipation. Compared to steel heat exchangers, AHE has lower flow resistance, which is beneficial for improving the overall effective energy efficiency of the system.

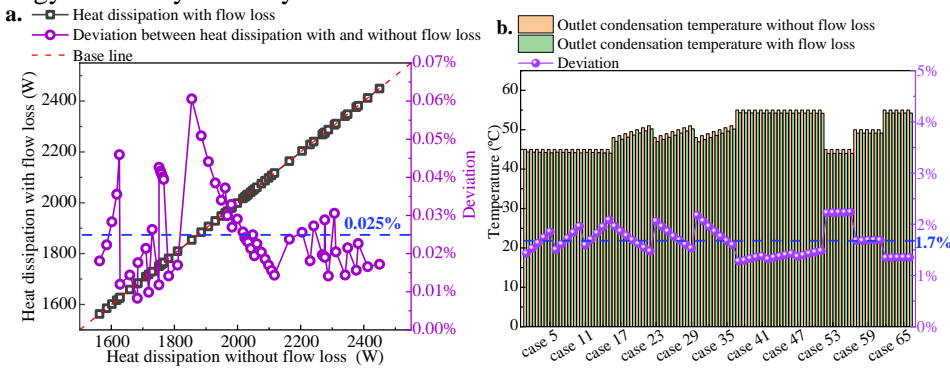


Figure 8: Flow loss analysis in 66 numerical cases: effects on heat dissipation (a) and effects on outlet condensation temperature (b).

3.4 THERMOLYSIS CORRELATION OF AHE

Based on the characteristic formula of the heat dissipation of the radiator [30], the thermolysis correlation of AHE heat dissipation related to inlet condensation temperature, the indoor air temperature, and the building envelope temperatures are defined as follows:

$$q = A \Delta t_a^B \Delta t_b^C \quad (8)$$

$$\Delta t_a = t_{con} - t_{ai} \quad (9)$$

$$\Delta t_b = t_{con} - t_{AUST} \quad (10)$$

where q is the heat flux, W/m^2 . G_{re} is the refrigerant flow rate, kg/h . t_{con} is the inlet condensation temperature, °C. t_{ai} is the indoor air temperature, °C. t_{AUST} is the comprehensive average temperature of the building envelope, °C. Δt_a is the difference between the inlet condensation temperature and the indoor air temperature, °C. Δt_b is the difference between the inlet condensation temperature and the building envelope temperature. A , B and C are fitting constants.

Based on the numerical results, the thermolysis correlation for the heat dissipation of the AHE is fitted with the least squares method, which is given as follows:

$$q = 113.281 \Delta t_a^{0.7105} \Delta t_b^{0.1215} \quad (11)$$

The deviation of the fitted correlation changes from -7.1% to 3.9%, with an average absolute deviation of 1.92% and an R^2 of 0.9694. The application of the thermolysis correlation is: $45\text{ °C} \leq t_{\text{con}} \leq 55\text{ °C}$, $2\text{ °C} \leq \Delta t_{\text{re}} \leq 10\text{ °C}$, $18\text{ °C} \leq t_{\text{ai}} \leq 22\text{ °C}$, $14\text{ °C} \leq t_{\text{AUST}} \leq 18\text{ °C}$, $32\text{ kg/h} \leq G_{\text{re}} \leq 47\text{ kg/h}$.

4. CONCLUSIONS

In this paper, an aluminum fanless thermal storage indoor heat exchanger (AHE) is proposed, which can be integrated with air source heat pump systems for clean indoor heating. The heat transfer and flow model of the AHE is established to analyze the thermal potentials of the AHE under multiple operation parameters. Finally, a thermolysis correlation for the AHE heat dissipation prediction was proposed. The main conclusions are as follows:

- 1) The thermal performance of the AHE is superior. The heat flux of the proposed heating terminal is as high as 2216.3 W/m^2 under the condensation temperature of 45.7 °C .
- 2) The deviations between the simulated and experimental data of the AHE heat dissipation and temperatures of each layer are all below 5%, verifying the reliability and effectiveness of the model.
- 3) The main operating parameter that affects the heat dissipation of the AHE is the inlet refrigerant pressure, while the main operating parameter that affects the pressure drop of the AHE is the refrigerant flow rate. The average temperature difference between the copper tube and the water layer is 6.3 °C , and the temperature difference between the fin end and the indoor air is 17.6 °C . Therefore, the heat transfer efficiency of the AHE can be further improved by reducing the thickness of the water layer and increasing the length of the fins.
- 4) The average absolute deviation of the proposed thermolysis correlation is 1.57%, and the goodness of fit R^2 is 0.9694. The thermolysis correlation contributes to the promotion and application of novel indoor heat exchangers.

Nomenclature

A	Area (m^2)	α	Convective heat transfer coefficient $\text{W}/(\text{m}^2 \cdot \text{°C})$
AHE	Aluminum fanless thermal storage indoor heat exchanger	β	Coefficient of expansion ($1/\text{°C}$)
AUST	Comprehensive average temperature	δ	fin thickness (m)
COP	Coefficient of performance	Δl	Control volume length (m)
d	Diameter (m)	ζ	Void fraction
G	Refrigerant flow rate (kg/h)	θ	Excess temperature (°C)
Gr	Grashof number	λ	Thermal conductivity $\text{W}/(\text{m} \cdot \text{K})$
h	Enthalpy (J/kg)	μ	Dynamic viscosity (Pa·s)
L	Length (m)	ρ	Density (kg/m^3)
La	Laplace number	Subscript	
n	Fin number	ai	Indoor air
Nu	Nusselt number	ap	Aluminum panel
PMV	Predicted mean vote	bu	Building envelope
PPD	Predicted percentage of dissatisfied	co	Copper tube
Pr	Prandtl number	con	Condensation temperature
P	Pressure (kPa)	cond	Conduction
Q	Heating dissipation (W)	conv	Convection
q	Heat flux (W/m^2)	fi	Fins
Ra	Rayleigh number	in	Inlet
Re	Reynolds number	out	Outlet
s	Surface area (m^2)	rad	Radiation
v	Gas specific volume (m^3/kg)	re	Refrigerant
We	Weber number	wa	Water
x	Refrigerant dryness (kg/kg)		

ACKNOWLEDGEMENT

This study was supported by the “Pioneer” and “Leading Goose” R & D Program of Zhejiang (2025C02239) and the scientific research fund of Zhejiang Sci-tech University (No. 21052322-Y).

REFERENCES

- [1] International Energy Agency. IEA (2023), *Energy Statistics Data Browser*, IEA, Paris <https://www.iea.org/data-and-statistics/data-tools/energy-statistics-data-browser>.
- [2] Zhao X, M X W, Chen B Y, Shang Y P, Song M L. Challenges toward carbon neutrality in China: Strategies and countermeasures [J]. *Resources, Conservation and Recycling*, 2022, 176, 105959.
- [3] Tanabe S, Kimura K. Importance of air movements on thermal comfort under hot and humid conditions [C]. *Proceedings of the Second ASHRAE Far East Conference on Air Conditioning in Hot Climates, Kuala Lumpur: ASHRAE*, 1989, 95-103.
- [4] Chen shouhai, Gao tong, Wang jun, Wang hongchao. Research on temperature field characteristics and thermal comfort of wall type frequency conversion air conditioner [J]. China Academic Journal Electronic Publishing House. 2018, 147-151.
- [5] HUANG Yunqi, SITU Shan shan, CHEN Xiaohui. Experimental Study on Optimal Air Temperature for Wall-Mounted Air Conditioning Heating Comfort [J]. *Environmental Technology*, 2019, 37(03): 64-69.
- [6] Olesen B. Comparative Experimental Study of Performance of Radiant Floor- Heating Systems and a Wall Panel Heating System Under Dynamic Conditions [J]. *ASHRAE Transactions*, 1994, 100(1): 1011-1023.
- [7] Xiao B, He L, Zhang S H, et al. Comparison and analysis on air-to-air and air-to-water heat pump heating systems [J]. *Renewable Energy*, 2020, 146(2): 1888-1896.
- [8] Zhang H, Jiang L F, Zheng W D, et al. Experimental study on a novel thermal storage refrigerant-heated radiator coupled with air source heat pump heating system [J]. *Building and Environment*, 2019, 164(15): 106341.
- [9] Zeng zhangchuan. Thermodynamics Analysis and Heat Transfer Research of Direct Radiant Floor Heating System with ASHP [D]. China, Zhenzhou: Zhengzhou University, 2010.
- [10] Wang yuanyuan, Zhang chao, liang nianliang, et al. Research status of air source heat pump refrigerant direct heating system for building heating [J]. *Building Energy Efficiency*, 2015, 43(07): 21-24.
- [11] Dong J K, Zhang L, Deng S M, et al. An experimental study on a novel radiant-convective heating system based on air source heat pump [J]. *Energy and Buildings*, 2018, 158(1): 812-821.
- [12] Shao Suola, Zhang Huan, You Shijun, Wang Yaran. Experimental investigation of air-source heat pump heating system with a novel thermal storage refrigerant-heated panel [J]. *Journal of Thermal Science and Engineering Applications*, 2021, 139(1): 011015.
- [13] Debabrata Pal, Nasim Hasan, Pabbathi Vijaya Rao, Nagarajan. Temperature distribution analysis of Cu, Al and steel material heat exchangers by ANSYS [J]. *Materials Today: Proceedings*, 2022, 56: 3176-3185.
- [14] He B H, Li L L, He G C. Experimental study on heat transfer performance of micro-grooved I-shaped aluminum heat pipe for heat pipe heat exchangers [J]. *Applied Thermal Engineering*, 2024, 253: 123733.
- [15] Arima H, Nishiguchi M, Suehiro S. Effect of the surface form of the herringbone aluminum plate in a plate heat exchanger on the boiling heat transfer performance of ammonia [J]. *Applied Thermal Engineering*, 2024, 256: 124057.
- [16] Guo X, Wei H B, He X, et al. Experimental evaluation of an earth-to-air heat exchanger and air source heat pump hybrid indoor air conditioning system [J]. *Energy and Buildings*, 2022, 256: 111752.
- [17] Yang J M, Cao H Q, Wang Z W, et al. Direct-supply chilled-water radiant-floor cooling system coupled with an earth-air heat exchanger system: A case study in a building [J]. *Case Studies in Thermal Engineering*, 2025, 65: 105586.
- [18] Shao S L, Xu C C. Performance Analysis of Novel Direct-Condensation Heating Panels Integrated with Air Source Heat Pump System on Thermal Economy and System Efficiencies [J]. *Energies*, 2024, 17(18): 4561.
- [19] Shao S L, Zhang H, You S J, et al. Thermal performance analysis of a new refrigerant-heated radiator coupled with air-source heat pump heating system [J]. *Applied Energy*, 2019, 247: 78-88.
- [20] Shao S L, Zhang H, You S J, et al. Prediction of thermal potentials of multi-panel refrigerant heated radiator based on a mathematical model considering refrigerant flow distribution [J]. *Energy & Buildings*, 2020, 228: 110446.
- [21] Gnielinski V. New equations for heat and mass transfer in turbulent pipe and channel flow [J]. *International Chemical Engineering*, 1976, 16: 359-368.
- [22] Dittus F W, Boelter L M K. Heat transfer in automobile radiators of the tubular type [J]. *International Communications in Heat & Mass Transfer*, 1985, 12(1): 3-22.
- [23] William A D, Pega H. Heat transfer and flow regimes during counter-flow steam condensation in flattened-tube air-cooled condensers [J]. *International Journal of Heat and Mass Transfer*, 2020, 147: 118930.
- [24] John H. *A heat transfer textbook, 4th edition* [M]. USA: Phlogiston Press, 2018: 141-160, 523-577.

- [25] Tari I, Mehrtash M. *Natural convection heat transfer from inclined plate-fin heat sinks* [J]. *International Journal of Heat and Mass Transfer*, 2013, 56(1-2): 574-593.
- [26] Kraus A D, Aziz A, Welty J. *Extended Surface Heat Transfer* [M]. USA: Library of Congress, 2001: 58-92, 170-193.
- [27] Yang ZQ, Gong MQ, Chen CF, Zou X, Shen J. Two-phase flow patterns, heat transfer and pressure drop characteristics of R600a during flow boiling inside a horizontal tube [J]. *Applied thermal engineering*, 2017(120), 654-671.
- [28] Moody L F. Friction factors for pipe flow [J]. *Transactions on ASME* 1944, 66: 671–684.
- [29] Kim S M, Mudawar I. Universal approach to predicting two-phase frictional pressure drop for adiabatic and condensing mini/micro-channel flows [J]. *International Journal of Heat and Mass Transfer*, 2012, 55(11-12): 3246-3261.
- [30] General Administration of Quality Supervision, Inspection and Quarantine of the People's Republic of China, National Standardization Administration of China. GB/T 13754-2017 *Test methods of thermal output of heating radiators* [S]. Beijing: China Standards Publishing House, 2018

Received: 27.5.2024.

Revised: 26.1.2025.

Accepted: 2.2.2025.